Simulation of Impulse Noise Suppression in a Powerline Connection

Undergraduate Thesis

Submitted in partial fulfillment of the requirements of the Bachelor's Thesis

By

Biruk Amare

Under the supervision of:

Prof. Dr.-Ing. Werner Henkel

JACOBS UNIVERSITY

August 2018

Declaration of Authorship

I, **Biruk Amare**, declare that this Undergraduate Thesis titled, '**Simulation of Impulse Noise Suppression in a Powerline Connection**' and the work presented in it are my own. I confirm that:

- This work was done wholly or mainly while in candidature for a research degree at this University.
- Where any part of this thesis has previously been submitted for a degree or any other qualification at this University or any other institution, this has been clearly stated.
- Where I have consulted the published work of others, this is always clearly attributed.
- Where I have quoted from the work of others, the source is always given. With the exception of such quotations, this thesis is entirely my own work.
- I have acknowledged all main sources of help.
- Where the thesis is based on work done by myself jointly with others, I have made clear exactly what was done by others and what I have contributed myself.

Signed: _____

Date: _____

Jacobs University Bremen

Abstract

Bachelor of Sciences (BSc.)

Simulation of Impulse Noise Suppression in a Powerline Connection

by **Biruk Amare**

In Power Line Communication (PLC) systems that use multi-carrier modulation, reduction of the influence of impulse noise is a challenging problem. To deal with this problem, in this thesis, we investigate the performance of an approach to mitigate the effects of impulse noise in PLCs. This approach uses a Normalized Least Mean Squares (NLMS) canceler which takes as reference input Neutral-Protective Earth (N-PE) pair signals and subtracts the filtered noise from the Live-Neutral (L-N) pair. Using such a canceler, the effects of the impulse noise that interferes with the direct (L-N) channel was tested for effective suppression. A Discrete Multi-Tone (DMT) transmission scheme, embedding the NLMS canceler as its channel, was devised. The Bit Error Ratio (BER) and Signal-to-Noise Ratio (SNR) performance of the DMT system using the proposed canceler was evaluated. Simulation results show the effectiveness of the proposed method.

Contents

Chapter 1

Introduction

Power Line Communication channels (PLCs) are often degraded by impulse noise, which is characterized by high amplitudes and random inter-arrival times. Cancellation/suppression of such noise is essential as it is the most damaging disturbance in a power line environment [11].

In [7], cancellation of impulse noise was investigated using the Common Mode-Differential Mode signals' relationship. This approach uses a Normalized Least Mean Squared (NLMS) algorithm to suppress the noise. The NLMS adaptive canceler takes a reference input, the common mode signal, and subtracts the adapted version from the differential mode signal. The effect of different parameters on the quality of the canceler was also investigated.

The suppressed output of the NLMS canceler was found to be adequate and performance-wise better than other canceler structures. This makes the NLMS canceler also attractive for our simulation. The aim of this work is therefore to check the performance of the NLMS algorithm in a Discrete Multi-Tone (DMT) multi-carrier power line communication system. As part of its channel, the DMT system embeds the adaptive algorithm to perform the cancellation. The algorithm makes use of the correlations of impulse-noise on Live-Neutral (L-N) and Neutral-Protective Earth (N-PE) pairs, allowing to use the N-PE signals as a reference to cancel the impulse noise from the other pair. This is implemented in a HomePlug-AV environment with predefined parameters for transmit signal, modulation and receiver structure. For other environments, the idea can directly be extrapolated, by changing the parameters and measurements.

This thesis is organized as follows. The first part of the report presents a background in the concept and characterization of Power Line Channels, transfer function measurements, crosstalk relationship, and impulse noise. The following Chapter 3 discusses multi-carrier modulation and its implementation. This is then followed by Homeplug-AV and power line standards. In Chapter 5, the simulation setup is presented. This is a thorough description of the project. Then, simulation results are presented in Chapter 6. This Chapter gives a discussion of the

contribution of our work and addresses the current results. It concludes on what is found and points to possible future works.

Chapter 2

Power Line Channel

Power Line Communication represents a formidable challenge of transmitting data along a communication media that was originally designed for the transmission of electrical energy [6]. From a three-wire configuration, the power line channel has two channels used for transmit and receive. As illustrated in Fig. 2.1, the first channel is the connection between the Live, which carries electric current, and the Neutral, which is usually at zero volts. This is termed as L-N. The second channel is from the Neutral to the Protective Earth, which has very low resistance, and forms a safety outlet. The second pair is abbreviated as N-PE or N-E.

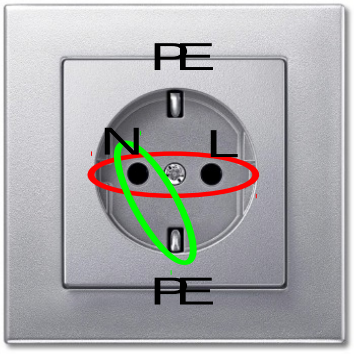

FIGURE 2.1: Power Line channels.

Characteristics of the illustrated pairs are often represented using transfer functions.

2.1 Transfer Function Measurement

The transfer function of the two channels can be measured using a vector network analyzer and an interface circuit designed for the measurement of such characteristic. The interface circuitry was installed in a special plug package and connected to the network analyzer. The characteristics of the L-N and N-PE channels are presented in Fig. 2.2.

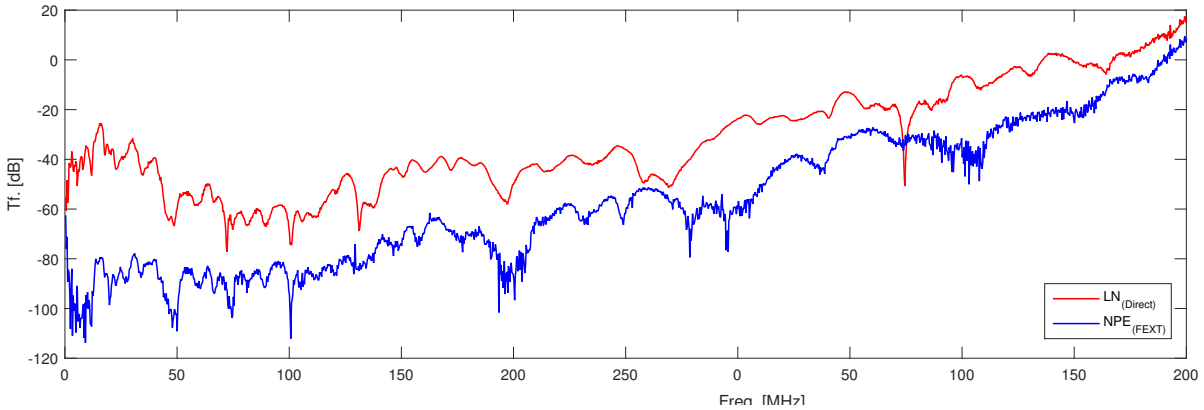

FIGURE 2.2: Transfer Function Measurements.

Coupling between wire pairs is present. For this project, we make use of the coupling correlation. For some frequencies, the shapes of the transfer functions are similar due to the same underlying topology of the different Multiple input multiple output (MIMO) paths [9].

2.2 Interferences in the Power line channel

There are three types of noise that affect the performance of a power line channel.

Crosstalk

Crosstalk is the unwanted coupling between two or mode adjacent lines. Fig. 2.3 shows the illustration of crosstalk in a twisted cable. The pair causing the interference is referred to as the "disturing pair' while the pair impacted by the crosstalk is the "disturbing line".

Crosstalk is distinguished as Near End Crosstalk (NEXT) and Far End Crosstalk (FEXT). **NEXT** is the disturbance at the receiver front end of a particular transceiver that is caused by signals transmitted by other transceivers at the same end of the cable.

FEXT is the interference at the receiver front end of a particular transceiver that is caused by signals transmitted by other transceivers at the opposite end of the cable.

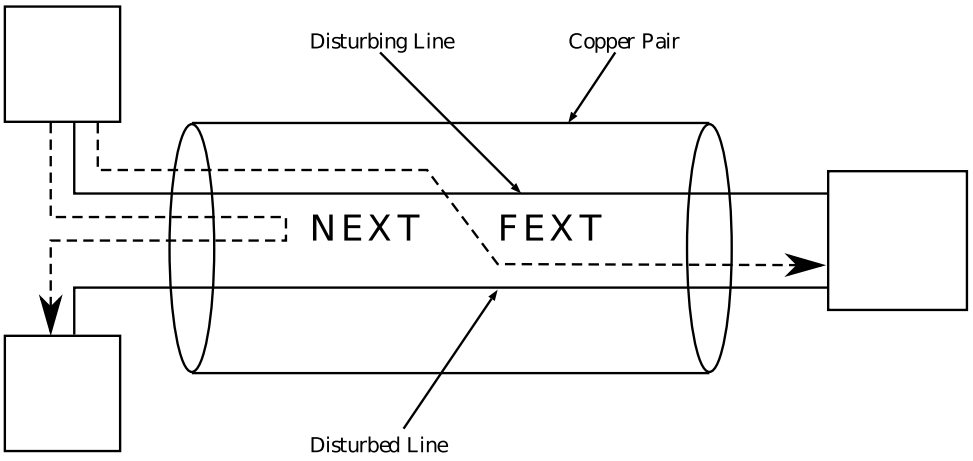

FIGURE 2.3: Crosstalk illustration.

Impulse Noise

Impulse noise events are random impulses with magnitudes that are so high that their presence can be associated with receiver detection errors. Impulse noise is characterized as a random pulse waveform whose amplitude is much higher than Gaussian-like background noise [3]. Fig. 2.4 presents a typical impulse noise measurements from an in-house power line channel.

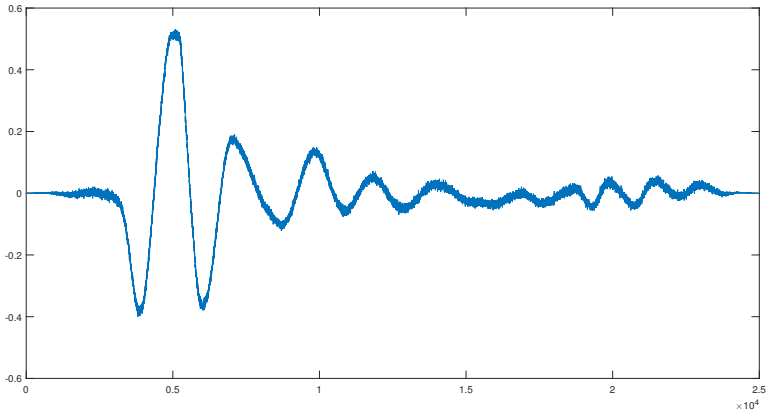

FIGURE 2.4: Typical Impulse noise measurement.

Impulse noise is essentially non-Gaussian. The reason why the Gaussian distribution does not accurately estimate impulse noise is because impulse noise exhibits large amplitudes known as outliers that occur too frequently to fit a Gaussian model.

Background Noise

Noise interference in PLCs that fits into a Gaussian probability distribution model is background noise. This summarizes resistive noise and a mixture of diverse interferences not specified

otherwise.

Chapter 3

Multi-carrier Communications

A digital communication system is composed of a transmitter, a receiver, and a channel. Multi-carrier modulation, particularly, has been successfully applied to a wide variety of digital communications applications over the past several years. The basic idea behind multi-carrier transmission is using several, mutually orthogonal and longer sinusoidal transmit wave forms.

3.1 OFDM/DMT

In Orthogonal Frequency Division Multiplexing (OFDM), multiple users can be granted access (multiplexed) to a channel with full orthogonality under the following popular conditions.

1. The sinusoids of orthogonal sets must be centered at frequencies multiple of the fundamental frequency.
2. The inverse of sub-channel spacing of each sub-carrier must be equal to the symbol duration, i.e, the sub-carrier spacing equals the inverse of the symbol period.

Discrete Multi-Tone (DMT) is fundamentally similar to the implementation of OFDM, used in a wireless environment, but in a wire-line environment. In contrast to OFDM, DMT has real-valued baseband multiplex, and the channel is known at the transmitter. It uses the available bandwidth, splitting into a number of sub-channels. This optimally utilizes channel capacities. In frequencies corresponding to significantly bad SNRs, carriers might be "turned-off" completely.

Fig. 3.1 presents a basic DMT transmission scheme. The input data of length $N/2$ is conjugate transposed to get the complete input data $\{x_0, x_1, x_2 \cdots, x_N\}$ to be converted to time-domain representation using the Inverse Discrete Fourier Transform (IDFT). Time-domain conversion is followed by a cyclic extension block to make the channel convolution appear cyclic. After

the channel convolutions, the cyclic extension is removed and the symbol is converted to DFT domain using the Discrete Fourier Transform (DFT).

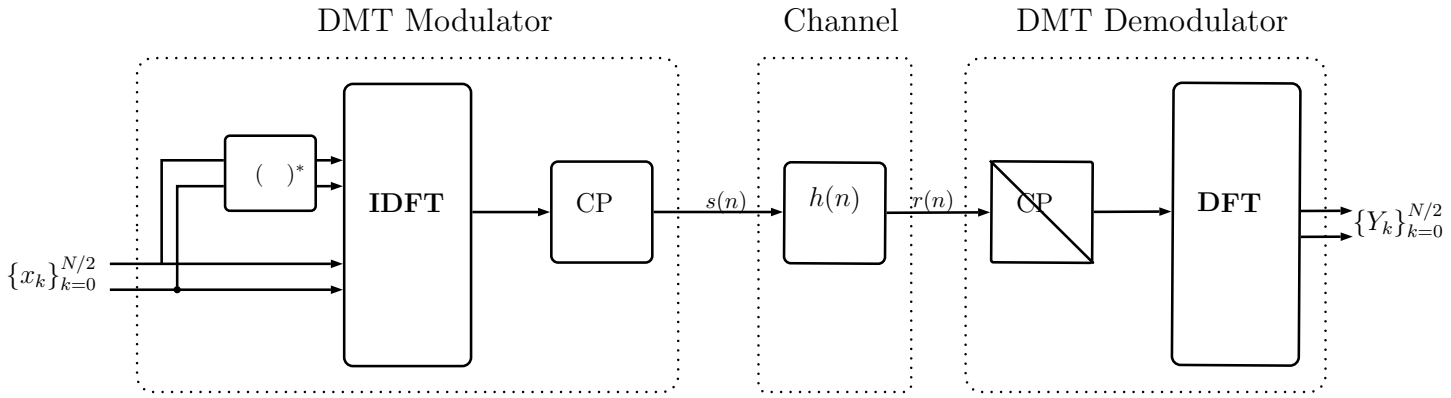

FIGURE 3.1: DMT Transmission.

In the above scheme:

$$x_0 = x_{N/2} = 0 \tag{3.1}$$

$$x_{N-k} = x_k^* \qquad k = 1, \cdots, N/2 - 1 \tag{3.2}$$

$$s(n) = IDFT_N\{x_k\}_{k=0}^{N-1} \qquad n = 0, \cdots, N-1 \tag{3.3}$$

$$s(n) = s(n+N) \qquad n = -L, \cdots, -1 \tag{3.4}$$

$$r(n) = h(n) \otimes s(n) \qquad n = 0, \cdots, N-1 \tag{3.5}$$

$$Y_k = DFT_N\{r(n)\}_{n=0}^{N-1} \qquad k = 0, \cdots, N/2\,, \tag{3.6}$$

where N is the DFT length, L is the length of the cyclic extension, $s(n)$ is the transmitted signal, $h(n)$ is the channel impulse response, and $r(n)$ is the received signal to be demodulated.

DMT Hermitian Symmetry

To guarantee a real-valued output for the transmit signal, we restrict the transmit symbols to obey conjugate symmetry.

$$x_k^{(i)} = x_{N-k}^{(i)} \qquad \text{and} \qquad x_k^{(q)} = -x_{N-k}^{(q)}\,, \tag{3.7}$$

which implies $x_0^{(q)} = x_{N/2}^{(q)} = 0$ and $x_0^{(i)} = x_{N/2}^{(i)} = 0$ Here, $x^{(i)}$ represents the in-phase component of x, and $x^{(q)}$ represents the quadrature component of x. Eq. (3.7) ensures Hermitian symmetry of the transmit symbol blocks.

We also know that

$$\begin{aligned}\cos(2\pi\frac{k}{N}n) &= \cos(2\pi\frac{(N-k)}{N}n)\\ \sin(2\pi\frac{k}{N}n) &= -\sin(2\pi\frac{(N-k)}{N}n)\end{aligned} \tag{3.8}$$

So, for $n = -L, \ldots, N-1$

$$\begin{aligned}s(n) &= \frac{1}{\sqrt{N}}\sum_{k=0}^{N-1}(x_k^{(i)}\cos(2\pi\frac{k}{N}n) - x_k^{(q)}\sin(2\pi\frac{k}{N}n))\\ &\quad + j\frac{1}{\sqrt{N}}\underbrace{\sum_{k=0}^{N-1}(x_k^{(q)}\cos(2\pi\frac{k}{N}n) + x_k^{(i)}\sin(2\pi\frac{k}{N}n))}_{=0}\\ &= \frac{1}{\sqrt{N}}\sum_{k=0}^{N-1}x_k e^{j2\pi\frac{k}{N}n}\end{aligned} \tag{3.9}$$

On the interval $0, \ldots, N-1$, the transmit signal multiplex $s(n)$ is generated by the scaled N-point IDFT of the data symbols x_k.

3.2 Modulation

The central part of multi-carrier modulation are the IFFT and FFT used to modulate the transmit symbols and demodulate the receive signal. Each symbol is seen as a "sub-carrier", which are orthogonal to each other, and modulated independently.

The DFT, in the normalized case, is given as

$$Y_k = \frac{1}{\sqrt{N}}\sum_{n=0}^{N-1} r(n)\cdot W_N^{kn}, \qquad k = 0, 1, \ldots, N-1 \tag{3.10}$$

The IDFT, in the normalized case, is given as

$$s(n) = \frac{1}{\sqrt{N}}\sum_{k=0}^{N-1} x_k\cdot W_N^{-kn}, \qquad n = 0, 1, \ldots, N-1\ , \tag{3.11}$$

where $W_N = e^{-j2\pi/N}$

To represent the DFT in matrix form, let us re-initialize the signals as vectors:

$$\mathbf{r}_N = \begin{bmatrix} r(0) \\ r(1) \\ \vdots \\ \vdots \\ r(N-1) \end{bmatrix} \mathbf{Y}_N = \begin{bmatrix} Y(0) \\ Y(1) \\ \vdots \\ \vdots \\ Y(N-1) \end{bmatrix} \mathbf{s}_N = \begin{bmatrix} s(0) \\ s(1) \\ \vdots \\ \vdots \\ s(N-1) \end{bmatrix} \mathbf{X}_N = \begin{bmatrix} X(0) \\ X(1) \\ \vdots \\ \vdots \\ X(N-1) \end{bmatrix},$$

$$\mathbf{W}_N = \begin{bmatrix} 1 & 1 & 1 & \cdots & 1 \\ 1 & W_N & W_N^2 & \cdots & W_N^{N-1} \\ 1 & W_N^2 & W_N^4 & \cdots & W_N^{2(N-1)} \\ \vdots & \vdots & \vdots & \ddots & \vdots \\ 1 & W_N^{N-1} & W_N^{2(N-1)} & \dots & W_N^{(N-1)(N-1)} \end{bmatrix}$$

With these definitions, the N-point DFT may be expressed in matrix form as

$$\mathbf{Y}_N = \mathbf{W}_N \mathbf{r}_N \tag{3.12}$$

and the N-point IDFT as

$$\mathbf{s}_N = \frac{1}{N} \mathbf{W}_N^* \mathbf{X}_N \,, \tag{3.13}$$

The matrix $\mathbf{W}_N$ is the matrix of linear transformation, it is a symmetric matrix [10].

For applying FFT/IFFT of Cooley-Tukey type, the number of carriers needs to be a power of two. If the number of sub-carriers is not a power of two, then it is common to append zeros to the input block.

The receiver operations are essentially the reverse of those in the transmitter. A critical set of functions, however, are symbol synchronization and frequency domain equalization, which is trivial.

3.3 Cyclic Extension

Severe Inter-Symbol-Interference (ISI) and Inter-Carrier-Interference (ICI) can be caused due to long impulse response or wrong symbol synchronization (neighboring symbols smearing out into one another). This in turn leads to loss of orthogonality, ISI and ICI. A cyclic prefix is used to separate symbols and make the channel convolution appear cyclic. It is under assumption that the length of the prefix is sufficiently larger than the channel impulse response.

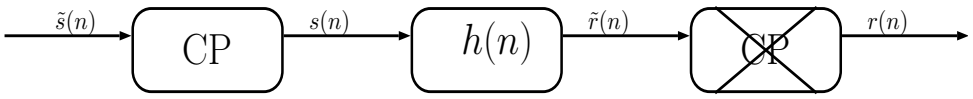

FIGURE 3.2: Cyclic Extension.

We describe the channel dispersion using a convolution matrix $\mathbf{H}$ linearly as:

$$\begin{bmatrix} r(0) \\ r(1) \\ \vdots \\ \vdots \\ \vdots \\ \vdots \\ r(N-1) \end{bmatrix} = \begin{bmatrix} h(L) & \cdots & h(1) & h(0) & 0 & \cdots & \cdots & \cdots & \cdots & 0 \\ 0 & \ddots & & h(1) & h(0) & \ddots & & & & \vdots \\ \vdots & & h(L) & \vdots & h(1) & \ddots & & & & \vdots \\ \vdots & & & h(L) & \vdots & \ddots & \ddots & \ddots & & \vdots \\ \vdots & & & 0 & h(L) & & \ddots & \ddots & \ddots & \vdots \\ \vdots & & & \vdots & \ddots & \ddots & & \ddots & \ddots & 0 \\ 0 & \cdots & \cdots & 0 & \cdots & 0 & h(L) & \cdots & h(1) & h(0) \end{bmatrix} \begin{bmatrix} s(-L) \\ \vdots \\ s(-1) \\ s(0) \\ s(1) \\ \vdots \\ \vdots \\ s(N-1) \end{bmatrix} \tag{3.14}$$

Here, we assume $L = M$, and M is the channel's impulse response. The first L received samples $\mathbf{r}(n), n = -L, \ldots, -1$ are implicitly ignored; CP removal.

We know that $\mathbf{s}(n) = \mathbf{s}(N-n), n = -L, \ldots, -1$, so we can write the convolution circularly as:

$$\underbrace{\begin{bmatrix} r(0) \\ r(1) \\ \vdots \\ \vdots \\ \vdots \\ \vdots \\ r(N-1) \end{bmatrix}}_{\mathbf{r}} = \underbrace{\begin{bmatrix} h(0) & 0 & \cdots & 0 & h(L) & \cdots & h(1) \\ h(1) & h(0) & \ddots & & 0 & \ddots & \vdots \\ \vdots & h(1) & \ddots & & \ddots & \ddots & h(L) \\ h(L) & \vdots & \ddots & \ddots & & & 0 \\ 0 & h(L) & & \ddots & \ddots & & \vdots \\ \vdots & \ddots & \ddots & & \ddots & \ddots & \vdots \\ 0 & \cdots & 0 & h(L) & & h(1) & h(0) \end{bmatrix}}_{\mathbf{H}} \underbrace{\begin{bmatrix} s(0) \\ s(1) \\ \vdots \\ \vdots \\ s(N-1) \end{bmatrix}}_{\mathbf{s}} \tag{3.15}$$

The convolution described above implicitly includes the addition and removal of the CP. It is only possible for $L \geq M$. The values highlighted in blue are the result of the CP being extended to the beginning of the signal in Eq. (3.14). The first L samples from the symbol after CP extension are the same as the last L samples of the same symbol before CP removal. In Eq. (3.15), the first L do hence not have to be listed in the vector $\mathbf{s}$ separately.

In the above representations, we assume that the cyclic prefix does not have a timing offset. For systems that have a cyclic prefix length that is not sufficiently larger than the channel impulse

response, a shortening time-domain equalization together with a suitable synchronization has to be in place.

3.4 Synchronization

Unlike single-carrier transmission in which a timing jitter can create ISI, a small timing offset does not violate orthogonality of transmitted waveforms in a multi-carrier systems [1]. Usually, the correlation between CP and the symbol is used for symbol synchronization. We simplify the task in our simulation, since synchronization is not what the scope of this thesis is.

We instead send a single impulse positioned at the beginning of the symbol and find the position of maximal energy in a window of length L. After this optimum window, we position the detection of length N, thereby eliminating the CP for subsequent symbols.

3.5 Equalization

Although not directly effective in single-carrier systems, zero-forcing algorithm is important in the implementation of equalization in DMT/OFDM receivers. The algorithm removes the ISI and ICI introduced by the transmission channel [8].

For a channel with frequency response $H(f)$, the zero forcing equalizer $C(f)$ is constructed by $C(f) = \frac{1}{H(f)}$. Thus, the combination of channel and equalizer gives a flat frequency response, $H(f)C(f) = 1$.

Chapter 4

Powerline Communications Standards

4.1 HomePlug AV

The HomePlug technology (PLC) provides a very simple and reliable way to connect devices to the Internet and one another using electrical wiring. The HomePlug system is specified for in-home communication adapted to the power line channel. It significantly enhances the capability to accommodate new generation of multimedia applications [9]. The HomePlug AV2 (latest version of the HomePlug technology) specification incorporates Multiple-Input Multiple-Output (MIMO) capabilities to improve throughput and coverage. Within a three-wire configuration, HomePlug AV2 uses a combination of any pairs for transmit and receive signals. In this thesis, the configurations presented in Chapter 2 was used.

The HomePlug AV2 DMT/OFDM parameters correspond to a system with 4096 carriers in a 100 MHz bandwidth, out of which 3455 carriers are only used from 1.8 to 86.13 MHz. The sub-carrier spacing of $24.414KHz$ was chosen in the Homeplug AV system. The specification also incorporates MIMO capability with 8192-point FFT's and has a guard interval or cyclic prefix length of 1920 samples.

In [9], the measurement campaigns for the extension of the frequency band up to 86 MHz is presented. Within the specification, it is listed that it is possible to provide flexibility in choosing the stop frequency in the $30 - 86$ MHz frequency band. The influence of windowing on Spectrum and Notch shape was also discussed. With different roll-off factors, the spectrum changes accordingly. The higher the roll-off factor of the raised-cosine window, the higher the attenuation achieved inside the notches and the narrower the notches in frequency will be. In this specification, using a roll-off factor of 0.1066, some guard carriers have to be omitted to

guarantee the depth of the notch. The roll-off factor, and the spectrum result in wasted resources that are possible to regain.

Power Spectral Density limits presented in the specification are based on the statistics of the impedance match at the interface between the device port and the varying and frequency-selective power line network.

Chapter 5

Impulse Noise Cancellation with Adaptive Filtering

5.1 Simulation Setup

The following simulation is performed using Matlab to check the performance of the DMT transmission scheme.

Data Generation

In this thesis, uniformly distributed random data was generated for transmission. The generated random pairs were mapped onto a complex plane as shown in Fig. 5.1. These points were to be modulated using the DFT as described in Chapter 3. The DFT length was chosen to be 8192-points. We used carriers from 73 to 3528 corresponding to 6910 carriers after conjugate extension, when for simplicity, we applied 4-QAM. The carriers corresponding to frequencies below 1.8 MHz and above 86.13 MHz in the 100 MHz bandwidth were not used.

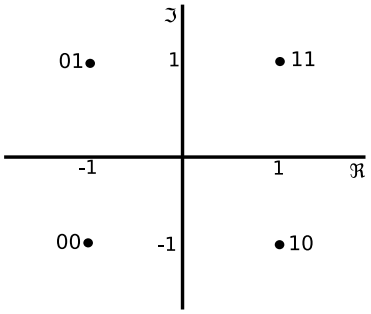

FIGURE 5.1: Constellation Points of generated data.

Our initial mapped vector of transmit symbols, using the DMT/OFDM conjugate symmetry property, was conjugate transposed to form the complete vector $\mathbf{X} = [0, 1.8\,\text{MHz} - 86.13\,\text{MHz}, 0, \cdots, 0, 86.13\,\text{MHz} - 1.8\,\text{MHz}, 0, \cdots, 0]$.

Up-sampling

The transmitted symbols then had to be oversampled to sufficiently represent the analog signal. The symbol to be modulated was oversampled by a factor of 4. This was easily done by padding zeros of length 25857 between $\mathbf{X}_{N-k}$ and its conjugate extension to have an overall symbol with a length of $32768 = 4 \times 8192$ including the DC value at the beginning of the symbol. The sampling rate corresponding to the original signal is the sub-carrier spacing of the symbol which is 24.414 KHz. The sampling rate corresponding to the upsampled signal is then $24.414 \times 4 = 97.656\,\text{KHz}$.

Cyclic Prefix Extension

We used, as given in [9], a cyclic prefix length of 1920. In the oversampled case, this means prepending the last $4 \times 1920 = 7680$ samples to the beginning of the symbol.

5.1.1 Transfer Function and Impulse Response

The transfer function of our DMT scheme is the measurement described in Chapter 2. Firstly, the measured data was correctly calibrated using the corresponding measurement files for both channels. Since this is only a few thousand samples, the data were interpolated using cubic Spline interpolation. For this, Matlab uses a piecewise continuous curve, passing through each of the values in the table. There is a separate cubic polynomial for each interval, each with its own coefficients. The slope is continuous.

Our interpolated signal is not yet shaped, so we had to apply a windowing function. Particularly, the Raised Cosine (RC) window function described as Eq. (5.1) was used. This was applied to remove the jumps at the end of the signal segment by fading the values there to zero. This removes the jumps and thus keep the background in the spectrum that is related to the frequency content of the signal.

The windowing function, for a frequency ω, is given as:

$$F(\omega) = \begin{cases} 1 & ,\omega < \omega_c(1-\alpha) \\ 0 & ,\omega > \omega_c(1+\alpha) \\ \frac{1+\cos(\frac{\pi(\omega-\omega_c(1-\alpha))}{\alpha\omega_c})}{2} & ,\omega_c(1-\alpha) < \omega < \omega_c(1+\alpha) \end{cases} \tag{5.1}$$

, where ω_c is half the data rate.

The function windows the last $\alpha \times 244.26207$MHz samples. In our particular case, we used a roll-off factor of 0.3. That means the last 600 points are in the transition region. This corresponding output from the windowing was then conjugate transposed. This was then directly converted to time domain representation using the IFFT. To get the filter coefficients for the convolution of the transfer function with the signal that was transmitted, the output was cyclically shifted using a specified threshold to find both of the impulse response ends. If the output was above that threshold, then the longest consecutive zeros was checked for and stored together. We used a threshold of 0.06 based on the plot of the output.

After this, impulse response had to be shortened. To do so, the side lobes were dragged down to zero using the windowing function in time domain. From this point let us denote the output from such windowing as $\mathbf{w}(m)$, and the signal transmitted as $\mathbf{s}(n)$.

Convolution

The convolution of the transmitted signal $\mathbf{s}(n)$ with the the transfer function $\mathbf{w}(m)$ was done using a a realization of an FIR system. The operation of the FIR filter at sample n is given by the time domain difference equation:

$$\mathbf{z}(n) = \sum_{m=0}^{N-1} \mathbf{w}(m)\mathbf{s}(n-m) \tag{5.2}$$

5.1.2 Impulse Noise Addition

After convolution with each channel, i.e, direct and reference channel, the transmitted signal was disturbed by adding impulse noise. As mentioned in Chapter 2, the impulse noise is characterized by random inter-arrival times. For now, the noise is added at constant inter-arrival times. As shown in the following figure, the impulse noise measurements were added starting at inter-arrival spacing, T_i, which must be greater than the length of the Impulse noise to be added.

Background Noise

There are additional background disturbances that are present in actual power line communication channels. We recognize this as (AWGN) Additive White Gaussian Noise.

$$\mathbf{r} = \mathbf{y} + \mathbf{N} \, , \tag{5.3}$$

where as shown in Fig. 5.3, $\mathbf{y}$ is the signal, $\mathbf{N}$ is the AWGN, and $\mathbf{r}$ is the output after addition.

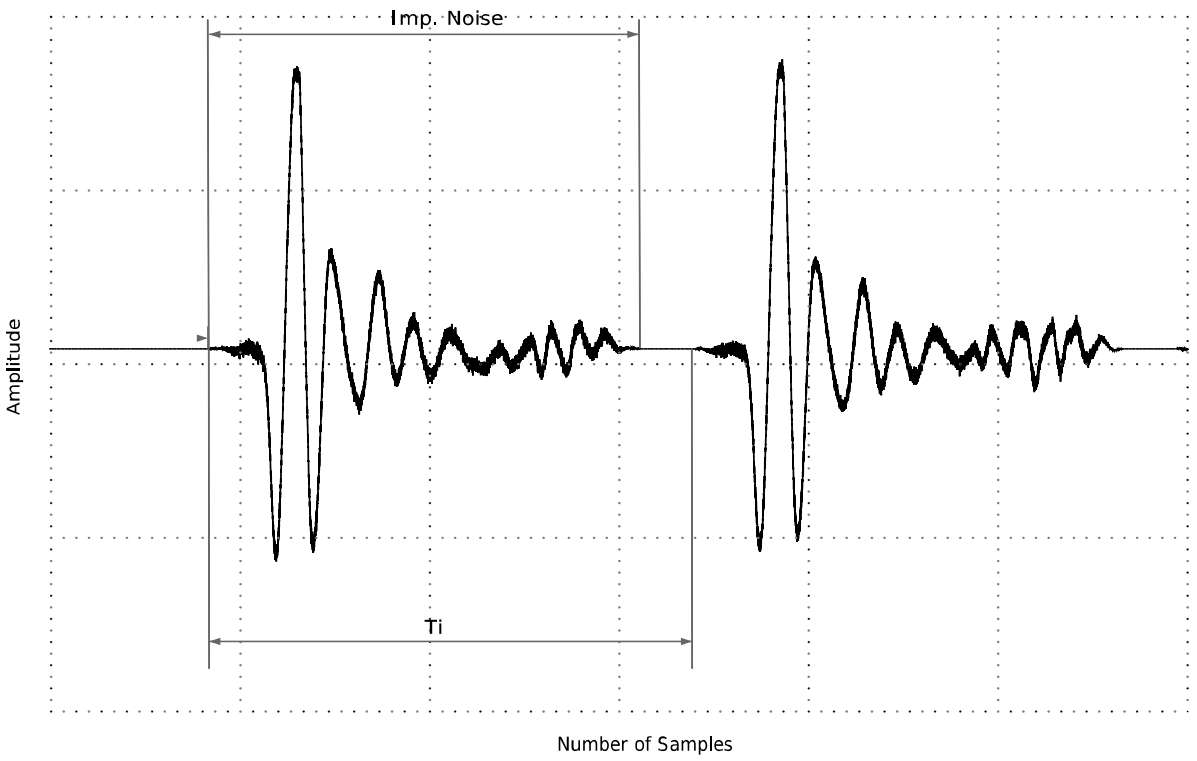

FIGURE 5.2: Impulse noise addition at inter-arrival times.

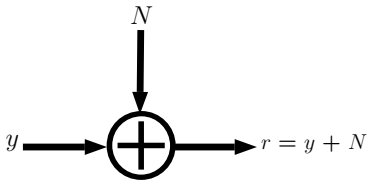

FIGURE 5.3: AWGN noise addition.

Receive/Anti-aliasing filter

Anti-aliasing filter is used to remove unwanted frequency interferences from the band of interest. For this simulation, a low-pass, Chebyshev Type-II, IIR filter with a passband frequency of 30MHz and a stopband frequency of 80MHz was used. This was an order-7, and 4 second order sections.

Down-Sampling

After the signal is anti-aliased using the filter presented in Fig. 5.4, it was then down-sampled, i.e., every 4^{th} sample was taken.

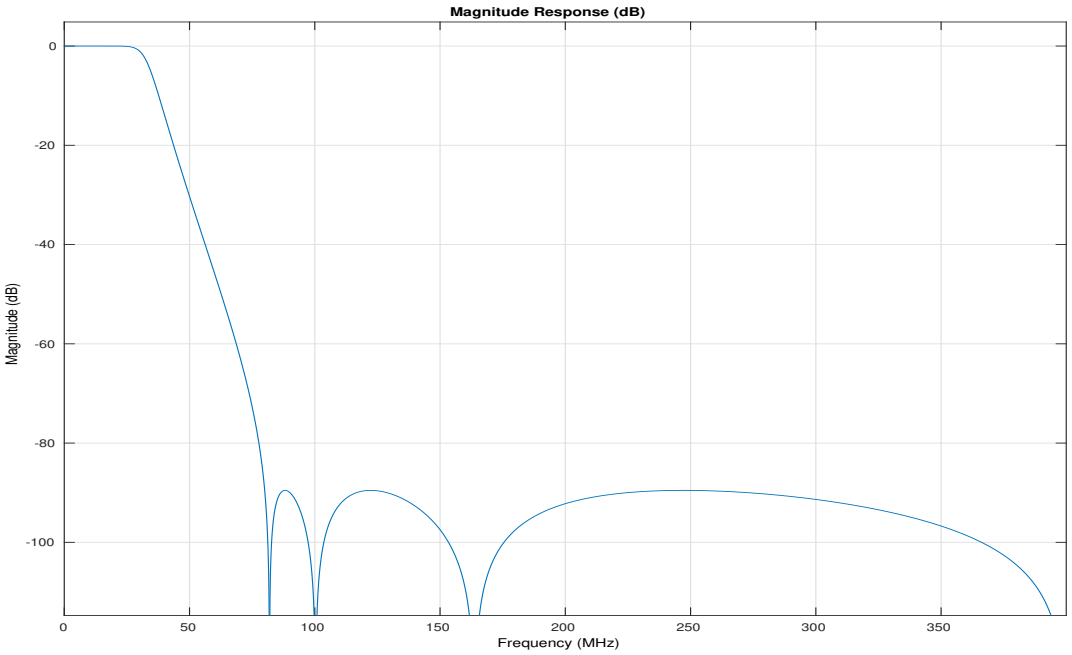

FIGURE 5.4: Anti-aliasing low pass filter.

5.1.3 Adaptive Filtering

The concept of adaptive filtering has found a lot of applications over the past 3 decades, ranging from channel equalization and echo cancellation to mitigation of narrow-band interference in wide-band signals [6].

The Least Mean Squares (LMS) algorithm is typically used due to its low computational complexity , robustness, and ease of implementation [12].

The LMS algorithm is a linear adaptive filtering algorithm, which consists of two basic components. A transversal filter which performs linearly filtering of the input signal and generates a signal which is to be compared with a desired output and an adaptive weight-control mechanism that adjusts the parameters of transversal filter using the estimated error.

The LMS filter involves feedback in its operation, stability is of critical importance. For the algorithm to converge, the mean-square error produced by the LMS filter, $J(n)$, must converge to its final value, $J(\infty) = constant$ as $n \to \infty$.

A block diagram is presented in Fig. 5.6. The tap input vector $\mathbf{U}(n)$ is an $M \times 1$ vector. The tap weight vector $\hat{\mathbf{w}}(n)$ is comprised of tap weights $\hat{w}_0(n), \hat{w}_1(n), \ldots, \hat{w}_{M-1}(n)$, which are initialized to zero, randomly if prior knowledge is not provided. $d(n)$ is the desired output at time n, where $\hat{d}(n|U_n)$ is the estimate of the desired output. Finally, the error is represented by $e(n)$ [6].

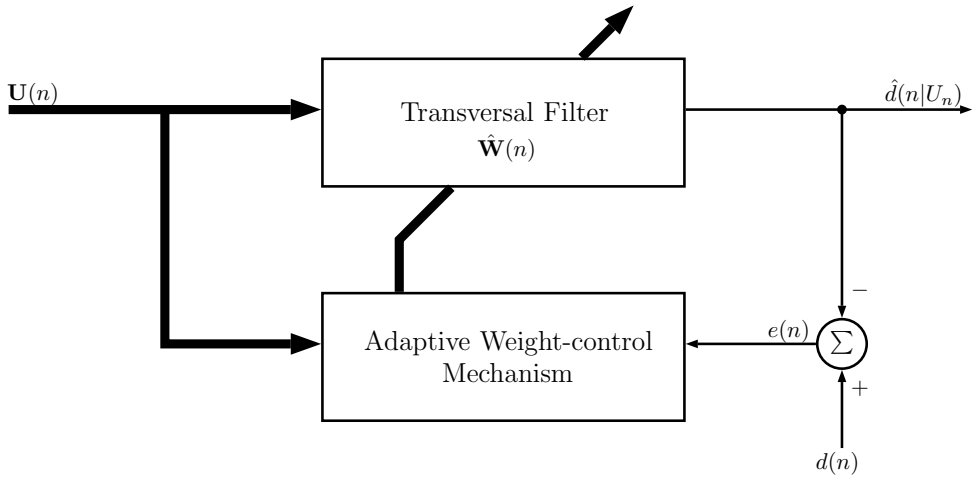

FIGURE 5.5: Block diagram of adaptive transversal filter.

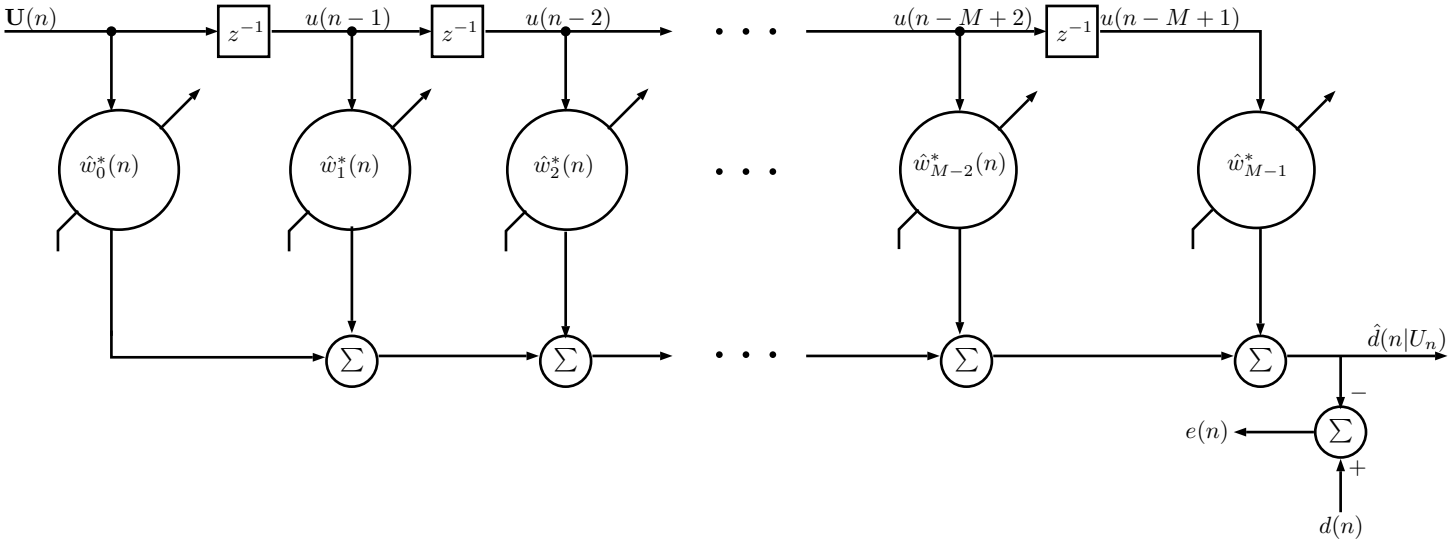

FIGURE 5.6: Detailed structure of the transversal filter component.

The output of the transversal filter is given by

$$\mathbf{y}(n) = \mathbf{w}^H(n)\mathbf{U}(n) \ , \tag{5.4}$$

The error is represented as

$$e(n) = d(n) - y(n) \tag{5.5}$$

And the adaptive weight control:

$$\hat{\mathbf{w}}(n+1) = \hat{\mathbf{w}}(n) + \mu\mathbf{U}(n)e^*(n) \ . \tag{5.6}$$

The second term of Eq. (5.8), $\mu\mathbf{U}(n)e^*(n)$ represents the adjustment on $\hat{\mathbf{w}}(n)$. The iteration starts with an initial guess $\hat{\mathbf{w}}(0)$.

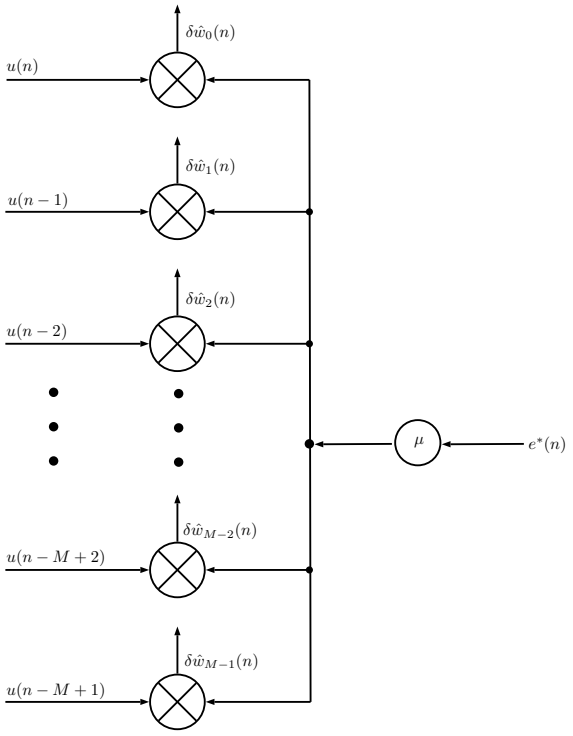

FIGURE 5.7: Detailed structure of the adaptive weight-control mechanism.

The Normalized LMS algorithm variant is defined as:

$$e(n) = d(n) - \hat{\mathbf{w}}^H(n)\mathbf{U}(n) \,, \tag{5.7}$$

$$\hat{\mathbf{w}}(n+1) = \hat{\mathbf{w}}(n) + \frac{\mu}{\|\mathbf{U}(n)\|^2}\mathbf{U}(n)e^*(n) \,, \tag{5.8}$$

where μ is a positive scaling factor and $\|\|$ is the Euclidean norm.

Using an optimum step size, the error will eventually converge to a minimum. The LMS algorithm has a computational complexity of $\mathcal{O}(M)$[7].

Impulse Noise Cancellation

As illustrated in Fig. 5.8, the filter structure of our impulse noise canceler uses two inputs. Since the LN and NPE channels are nicely correlated, the NLMS noise canceler was developed choosing the LN signal as the primary input and the NE signal as the reference input [4]. The algorithm computes the output (error) with reduced noise by subtracting the LN signal from the estimation. The error is then fed back to the adaptive filter to calculate the new tap weight vector. For initialization, tap weight vector was set to zero. The NLMS algorithm was gated when the impulse noise was exceeding a certain threshold. Output from the cancellation is presented in Chapter 5.2.

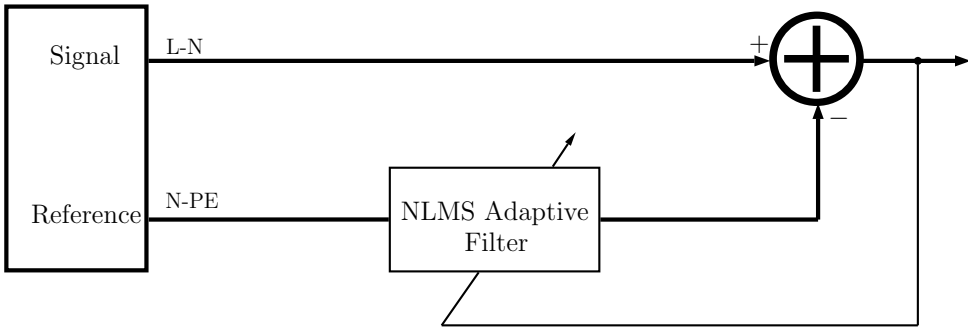

FIGURE 5.8: NLMS Adaptive Canceler

Cyclic Prefix Removal

In the transmitter, we had prepended a cyclic prefix. This was only to avoid ISI. Since our cyclic prefix is sufficiently large, we simply had to remove the prepended CP. For systems that have less cyclic prefix length, a synchronization method like the one described in Chapter 3 has to be used.

Zero-forcing Equalizer

To simplify our procedure in the simulation, we just send an all-ones vector in DFT domain and obtain the samples of the transfer function directly, which is used for the frequency domain equalizer.

$$C(f) = \frac{1}{E(f)} \ ,$$

where $E(f)$ is the received symbol and $C(f)$ is the inverse of the zero-forcing coefficient.

5.2 Simulation Results

The following results have been obtained after a successful iteration of the system for a sufficient number. After 200 iterations, the Bit-Error-Ratio is presented along with the Signal-to-Noise-Ratio distribution.

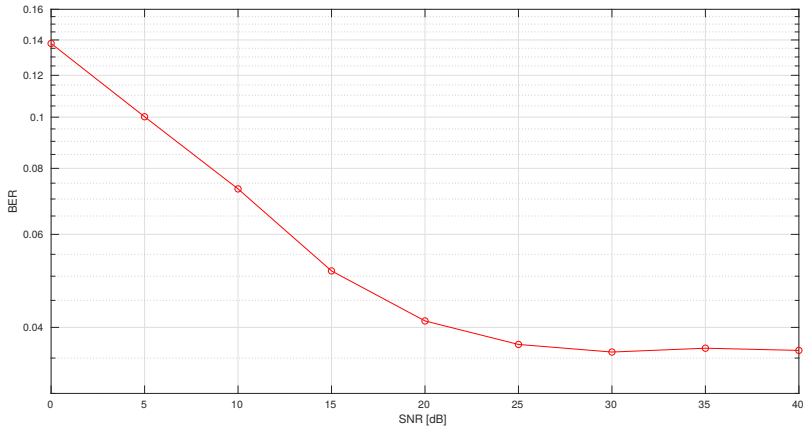

FIGURE 5.9: BER vs SNR distribution without cancellation is activated.

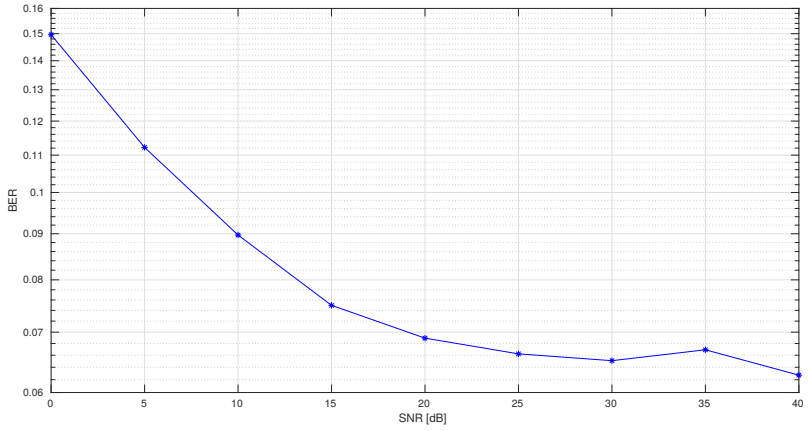

FIGURE 5.10: BER vs SNR distribution after cancellation is performed.

Due to wrong equalizer settings, the BER after the canceler is higher than the BER without the canceler. To fix this, one has to re-adjust the Zero-forcing equalizer to correspond to the output from the canceler. Since the canceler is gated to when there is Impulse Noise, the factor for equalization will not be constant.

Fig. 5.11 and 5.12 show the received symbol constellations for a background noise of SNR= 40dB.

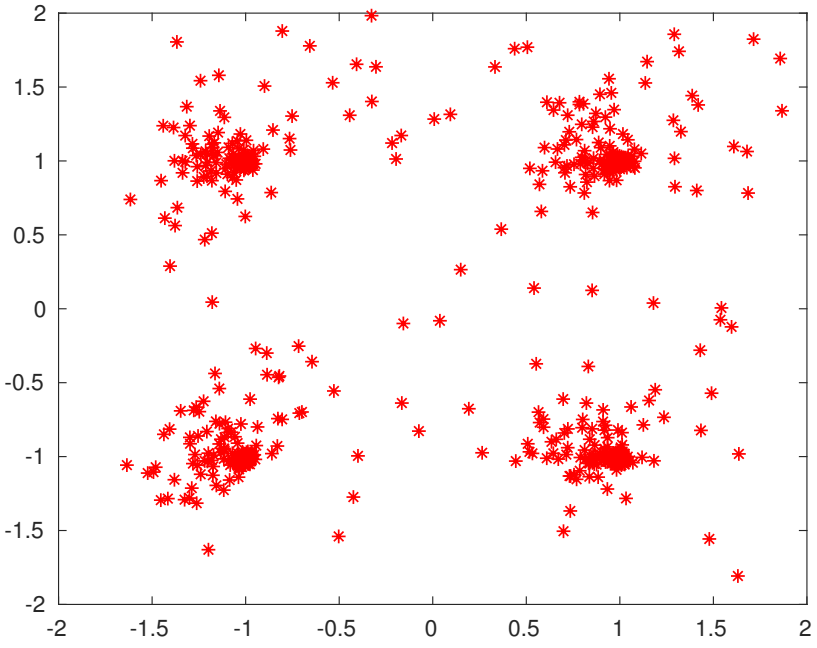

FIGURE 5.11: Received constellation before cancellation

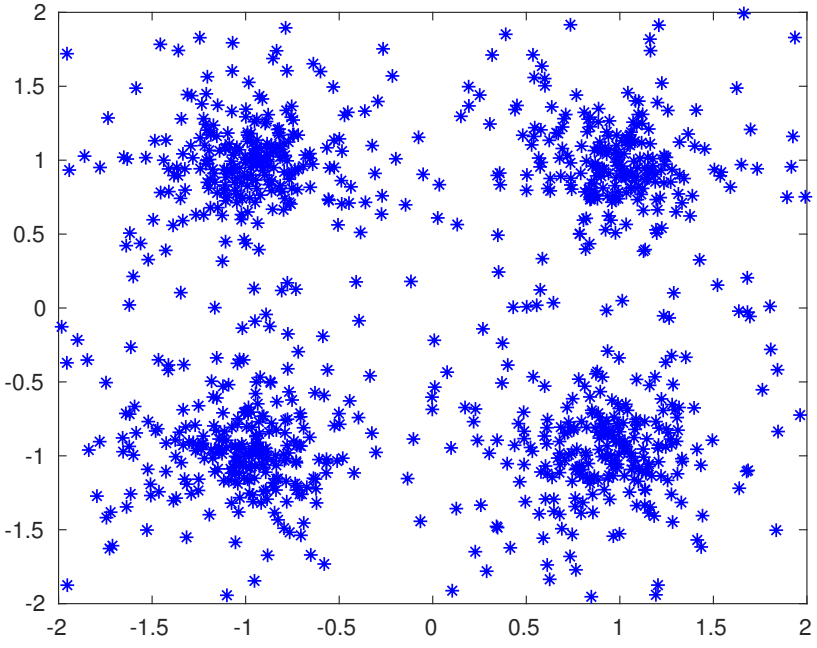

FIGURE 5.12: Received constellation after cancellation.

The points corresponding to the proper symbol are now converted to clouds around the point, which is the result of the equalization factor.

Although, the BER decision boundary is not attractive yet, the canceler successfully removes unwanted components like in the following figure.

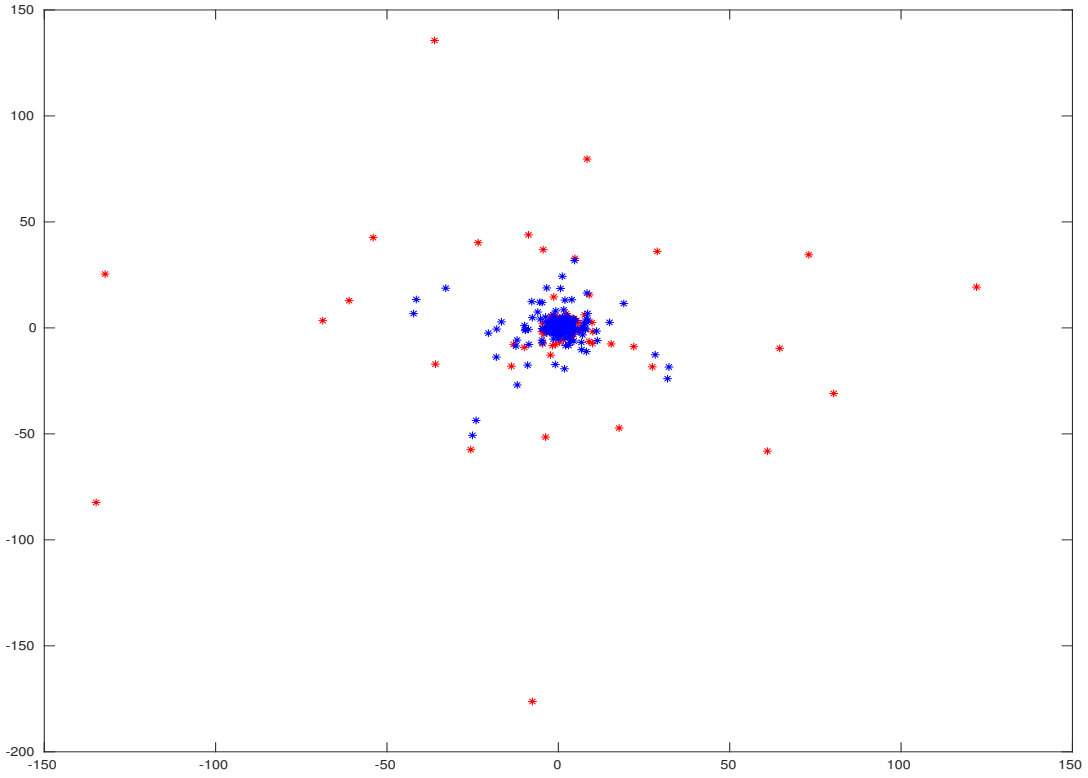

FIGURE 5.13: Received Symbols.

In the above figure, the red points are the received symbols before cancellation and the blue points are the received symbols after cancellation.

Chapter 6

Concluding Remarks

In this thesis, we have investigated the performance of an NLMS canceler in a DMT transmission scheme.

The first portion of this work concentrated on parameterizing and analyzing specifications for the DMT system. Then, through measurements, we realized the channel properties and the correlation between the LN and NPE wire pairs. Afterwards, we introduced the impulse noise measurements to the channels. Consequently, we analyzed filter structures, and the canceler structure and showed the properties. The simulation results showed that even after training the canceler for a sufficient number, a part of the original signal is canceled. One has to re-adjust the zero-forcing equalizer to adopt to the lost factor.

To conclude this thesis, although not optimal on the receiving end, the presented simulation serves as a detailed review for a possibly efficient system. With proper receive equalizer, an addition of Time-Domain-Equalizer (TEQ) and optimal detection method that involves efficient coding and error-correcting, the tested system can result in promising outputs.

Bibliography

[1] Ahmad R. Bahai and Burton R. Saltzberg. *Multi-Carrier Digital Communications: Theory and Applications of OFDM*. Plenum Publishing Co., 1999. ISBN: 0306462966.

[2] C. Cano et al. "State of the Art in Power Line Communications: From the Applications to the Medium." In: *IEEE Journal on Selected Areas in Communications* 34.7 (2016), pp. 1935–1952. ISSN: 0733-8716. DOI: 10.1109/JSAC.2016.2566018.

[3] Walter Y. Chen. *DSL: Simulation Techniques and Standards Development for Digital Subscriber Lines*. Alpel Publishing, 1997. ISBN: 1578700175.

[4] Oana Graur et al. "Impulse noise in DSL, powerline, and wireless". In: Darmstadt, Germany: Sitzung der ITG Fachgruppe "Angewandte Informationstheorie", Apr. 10, 2014. URL: http://trsys.faculty.jacobs-university.de/wp-content/uploads/2014/04/Impulse-Noise-ITG-Darmstadt.pdf. published.

[5] R. Hashmat et al. "MIMO communications for inhome PLC networks: Measurements and results up to 100 MHz." In: *ISPLC2010*. 2010, pp. 120–124. DOI: 10.1109/ISPLC.2010.5479897.

[6] Simon Haykin. *Adaptive Filter Theory (3rd Ed.)* Upper Saddle River, NJ, USA: Prentice-Hall, Inc., 1996. ISBN: 0-13-322760-X.

[7] Werner Henkel and Oana Graur. "Impulse Noise Cancellation based on the Common-Mode Signal." In: Princeton, NJ: 2010 IEEE Sarnoff Symposium, Apr. 12, 2010. URL: http://trsys.faculty.jacobs-university.de/wp-content/uploads/2014/02/sarnoff2010.pdf. published.

[8] T. Karp et al. "Zero-forcing frequency domain equalization for DMT systems with insufficient guard interval." In: *2003 IEEE International Conference on Acoustics, Speech, and Signal Processing, 2003. Proceedings. (ICASSP '03)*. Vol. 4. 2003, pp. IV–221. DOI: 10.1109/ICASSP.2003.1202599.

[9] Kaywan Afkhamie Larry Yonge Jose Abad. "An Overview of the HomePlug AV2 Technology". In: *Journal of Electrical and Computer Engineering* vol. 2013.1 (2013), pp. 88–99.

[10] John G. Proakis and Dimitris G. Manolakis. *Digital Signal Processing (3rd Ed.): Principles, Algorithms, and Applications*. Upper Saddle River, NJ, USA: Prentice-Hall, Inc., 1996. ISBN: 0-13-373762-4.

[11] Thokozani Shongwe, A J Han Vinck, and Hendrik Ferreira. "Broadband and Narrow-Band Noise Modeling in Powerline Communications." In: (Dec. 2015).

[12] B. Widrow et al. "Adaptive noise cancelling: Principles and applications." In: *Proceedings of the IEEE* 63.12 (1975), pp. 1692–1716. ISSN: 0018-9219. DOI: 10.1109/PROC.1975.10036.

[13] M. Zimmermann and K. Dostert. "Analysis and modeling of impulsive noise in broad-band powerline communications." In: *IEEE Transactions on Electromagnetic Compatibility* 44.1 (2002), pp. 249–258. ISSN: 0018-9375. DOI: 10.1109/15.990732.